Bio-Medical Materials and Engineering 26 (2015) S1431–S1438
DOI 10.3233/BME-151441
IOS Press

Geometric distortion evaluation using a multi-orientated water-phantom at 0.2 T MRI

Jochi Jao [a], Mingye Cheng [b], Hsintien Lee [b], Julius Ting [b] and Pochou Chen [c, *]
[a]*Department of Medical Imaging and Radiological Sciences, College of Health Sciences, Kaohsiung Medical University, 100, Shih-Chuan First Rd., Kaohsiung City, 80708, Taiwan, R.O.C.*
[b]*Department of Radiology, Antai Medical Care Cooperation Antai Tian-Sheng Memorial Hospital, No.210, Sec. 1, Zhongzheng Rd., Donggang Township, Pingtung County 928, Taiwan, R.O.C.*
[c]*Department of Biomedical Engineering, I-Shou University, No.8, Yida Rd., Jiaosu Village Yanchao District, Kaohsiung City, 82445, Taiwan, R.O.C.*

Abstract. Magnetic Resonance Imaging (MRI) has been one of the most revolutionary medical imaging modalities in the past three decades. It has been recognized as a potential technique in the clinical diagnosis of diseases as well as tumor differentiation. Although MRI has now become the preferred choice in many clinical examinations, there are some drawbacks, which still limit its applications. One of the crucial issues of MRI is the geometric distortion caused by magnetic field inhomogeneity and susceptibility effects. The farther the lesion from the center of a magnetic field (off-center field), the more severe the distortion becomes, especially in low-field MRI. Hence, it might hinder the diagnosis and characterization of lesions in the presence of field inhomogeneity. In this study, an innovative multi-orientated water-phantom was used to evaluate the geometric distortion. The correlations between the level of image distortion and the relative off-center positions, as well as the variation of signal intensities, were both investigated. The image distortion ratios of axial, coronal and sagittal images were calculated.

Keywords: Geometric distortion, field inhomogeneity, off-center field, multi-orientated water-phantom

1. Introduction

Magnetic Resonance Imaging (MRI) is an imaging modality that has revolutionized medical imaging in the past three decades, possessing the advantages of three-dimensional imaging capability with no ionizing radiation involved and is non-invasive over other imaging modalities. MRI has now become the preferred choice in many clinical examinations because of its superior capability of providing high contrast among soft tissues. It can differentiate not only abnormal tissue from normal tissue but different tissue types as well. However, the possibility of geometric distortion in MR images

* Address for correspondence: Pochou Chen, Department of Biomedical Engineering, I-Shou University, No.8, Yida Rd., Jiaosu Village Yanchao District, Kaohsiung City, 82445, Taiwan, R.O.C.. Tel.: +886937633143; Fax: +886761515150; E-mail: pcchen@isu.edu.tw.

somewhat limits its full potential for use in some clinical applications. Geometric distortion in MRI can be classified as hardware-related [1-3] and tissue-related [3-5]. The hardware-related geometric distortion from MRI hardware is mainly the inhomogeneity in the main magnet, the gradient field non-linearity, and the eddy currents induced by the switching of the gradient coils that are prominent in echo planar imaging (EPI). The tissue-related geometric distortion is mainly caused by susceptibility and chemical shift, which is imaging object-dependent. The image quality of MRI strongly depends on magnetic field strength and homogeneity [6-8]. Geometric distortion has long been regarded as a serious drawback of MRI. Geometric distortion caused by magnetic field inhomogeneity might not be readily depicted in high-field-strength MRI because the signal-to-noise ratio (SNR) is high. However, it will be notable in a low-field-strength MR scanner. In addition, it is found that the farther the region of interest is from the main magnet center, the more the geometric distortion [9]. For example, the MR images of a proximal femur and distal pelvis at 0.2 T are shown in Figure 1. Geometric distortions are clearly seen on both images. For MRI-based treatment planning for radiotherapy, high precision and accuracy is particularly required [6, 10]. A 3D multi-compartment phantom has been used to perform geometric distortion studies [9, 11]. Some 3D phantoms were used to study the effects of geometric distortion at 0.2 T and 1.5 T MRI respectively, in radiotherapy treatment planning of prostate cancer [12-15]. The geometric distortion is related to field-strength and homogeneity and regarded as an important issue in MRI. Hence, it would be valuable to evaluate the correlation among them. In this study, an innovative multi-orientated water-phantom was used for measurements of the geometric distortion. In contrast to other phantoms used to evaluate geometric distortions on MR images, this specially designed phantom is simple and feasible to obtain multi-circle images in all three orientations without repositioning the phantom. The correlations among the levels of image distortion related to the relative off-center position, as well as the variations of signal intensities, were investigated.

2. Materials and methods

An innovative multi-orientated water-phantom was designed in order to perform axial, coronal and sagittal scans. This is a parallelepiped tank without upper parallelogram made of 1-cm thickness Plexiglas, and the dimension was 30 cm (L) ×30 cm (W) ×21 cm (H). 3D water-phantom used to perform the quantitative assessment for related geometric distortion of the MR scanner is shown in Figure 2. In order to achieve multi-orientated purpose, the water-phantom included removable test plate slots to slide the specially designed experimental test plates. The dimensions of the two experimental test plates were 30 cm×20 cm for axial and sagittal and 30 cm×30 cm for coronal orientation. Both experimental plates were designed to have similar test patterns with 9×9 and 9×5 2D equally spaced circular holes. The diameter of each hole is 16 mm and the equal center-to-center distance between two adjacent holes is 32 mm. Components of multi-orientated water-phantom containing slotted water tank and two removable test plates are shown in Figure 3. The phantom was filled with a water solution doped with NiCl2· 6H2O (3.3685 g/L) and NaCl (2.4g/L).

The study was performed on a GE Signa Profile Excite 0.2-Tesla MR system (GE Medical Systems, Milwaukee, WI) which is an open low-field permanent magnet MR unit. The saddle type Body Flex II (L size) coil, a receive-only coil with 1.45 m diameter, was used to cover the entire water phantom. After 3-plane (axial, coronal and sagittal) localizer scan, T1 weighted images (T1WI) were obtained using 2D Gradient Echo pulse sequence. The scanning parameters were listed as follows: TR/TE = 100 ms/Min Full, $\alpha = 80°$, BW = 7.81 kHz, Matrix size = 256×256, NEX = 12, FOV = 40 cm, slice thickness = 5 mm. The scan time was 5 minutes and 10 seconds. The scans were performed under au-

to-shim mode. The tape and landmark laser light were used to adjust the location of the coil to ensure that the coil was in the center of the gantry. The A4 copy papers were used to adjust the experimental test plate in the water phantom to the center of the coil. Afterwards, the experimental test plate was put into the water phantom before MRI scans. In order to avoid the presence of artifacts caused by air bubbles on MR images, all the air bubbles in the water phantom were carefully removed. A custom program using MATLAB software was used to analyze the T1WI. The center coordinate displacements, circularity, geometric distortion, and SNR of circle holes were evaluated. Afterwards, SSPS statistical software was used to perform statistical analysis.

2.1. The center coordinate displacements of circle holes in x-axis (D_x), y-axis (D_y) and z-axis (D_z)

The definition of center coordinate displacement is the region of interest (ROI) center's coordinate of each circle hole on image subtracting the actual corresponding circle center's coordinate on Plexiglas as shown in Eq. (1). The MR images of multi-orientated water-phantom in three orientations are shown in Figure 4.

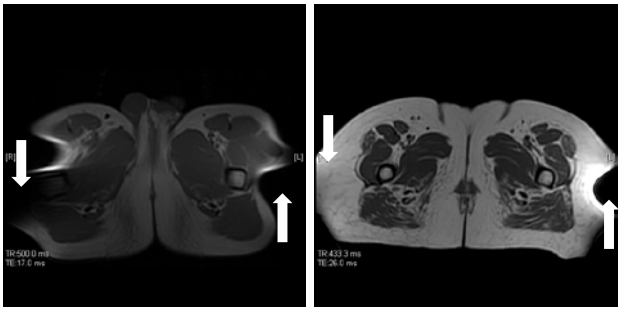

Fig. 1. MR images of proximal femur (left) and distal pelvis (right). White arrows show the areas of geometry distortion.

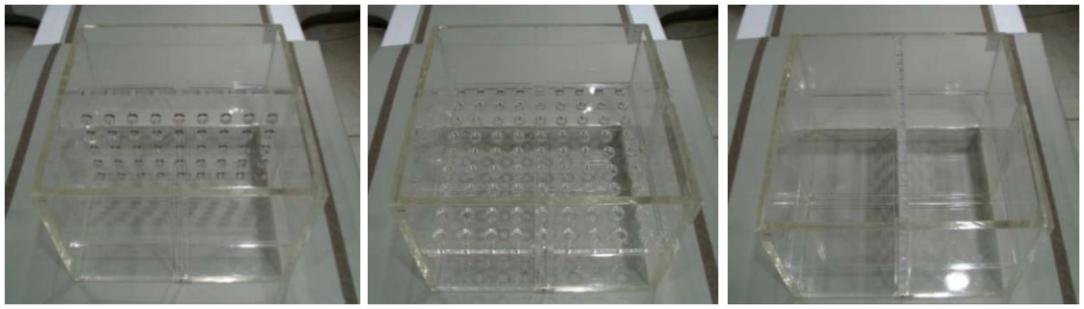

Fig. 2. Multi-orientated water-phantom in (a) axial (b) coronal and (c) sagittal configurations.

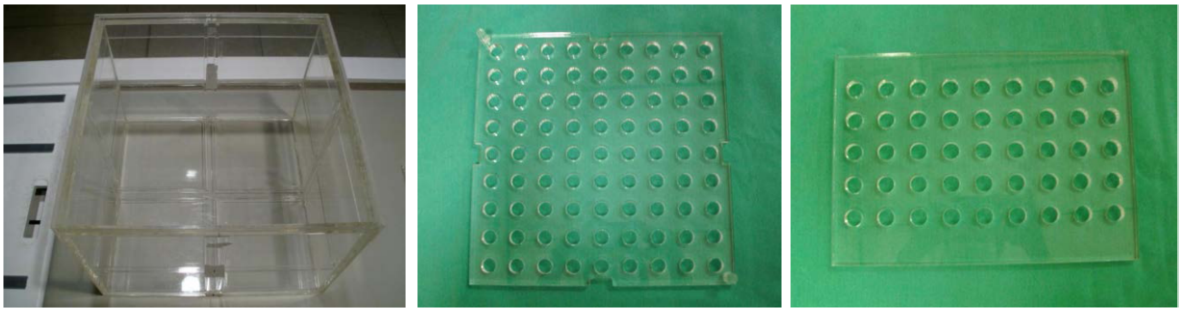

Fig. 3. Components of multi-orientated water-phantom containing slotted water tank and two removable test plates.

$$\begin{aligned} D_x &= x_i - x_{i0} \\ D_y &= y_i - y_{i0} \\ D_z &= z_i - z_{i0} \end{aligned} \tag{1}$$

whereas x_i, y_i and z_i are the ROI center's coordinate of each circle hole on images along the x-axis, x_{i0}, y_{i0} and z_{i0} are the actual corresponding circle center's coordinates on Plexiglas along the x-axis y-axis and z-axis, respectively.

2.2. Area distortion ratio (D_{Area})

The definition of Area distortion ratio is the ratio of ROI area of each circle hole to that of the center circle as shown in Eq. (2).

$$D_{Area} = \frac{A}{A_C} \times 100\%, \tag{2}$$

whereas A is the ROI area of each circle hole on images and A_C is the ROI area of center circle hole on images.

2.3. *Geometric distortion ratio (D_g) of the long axis and short axis*

The definition of geometric distortion ratio (circularity) is the ratio of the length of the short axis (i.e. shortest distance of two points on the circle and passing through the circle mass center) of each circle hole to the length of the long axis (i.e. longest distance) of each circle hole as shown in Eq. (3).

$$D_g = \frac{l_{long}}{l_{short}} \times 100\%, \tag{3}$$

whereas l_{long} is the length of the long axis of each circle hole on images and l_{short} is the length of the short axis of each circle hole on images.

2.4. SNR

The definition of SNR is the ratio of ROI value (i.e. average signal intensity) of each circle hole to the standard deviation of background circle's ROI as shown in Eq. (4).

$$SNR = \frac{ROI_C}{\sqrt{ROI_{BG}}}, \tag{4}$$

whereas ROI_C is the ROI value of each circle hole and ROI_{BG} is the standard deviation of background circle's ROI.

3. Results

3.1. Displacement of the center's coordinate

It was found that the distribution of magnetic field homogeneity tended to shift to the left along the x-axis, shift to the anterior along the y-axis, and shift to the inferior along the z-axis as shown in Figure 4. It was also found that the magnetic field homogeneity along the z-axis was superior. The displacements of the center's coordinate along x-axis, y-axis, z-axis respectively were in the range of -4.56 mm to +6.13 mm, -6.13 mm to +6.13 mm, and -2.3 mm to +2.31 mm, as shown in Table 1.

3.2. Area distortion ratio

It was found that the distortion ratio was in the range of 0.93-1.10 in the axial plane, 0.75-1.06 in the coronal plane and 0.89-1.10 in the sagittal plane as shown in Table 2.

3.3. Geometric distortion of the long axis and short axis

It was found that the circularity was in the range of 1.00-1.19 in the axial plane, 1.00-1.20 in the coronal plane and 1.00-1.12 in the sagittal plane as shown in Table 3.

3.4. Signal-Noise ratio

It was found that the largest ROI value was in the coronal plane, and was in the order of coronal > axial > sagittal as shown in Table 4. The box plots of SNR and center-displacements in three anatomically oriented slices as shown in Figure 5 were obtained by using SSPS statistical software. The SNR box plot clearly shows that the variation of SNR is different among the three orientated planes.

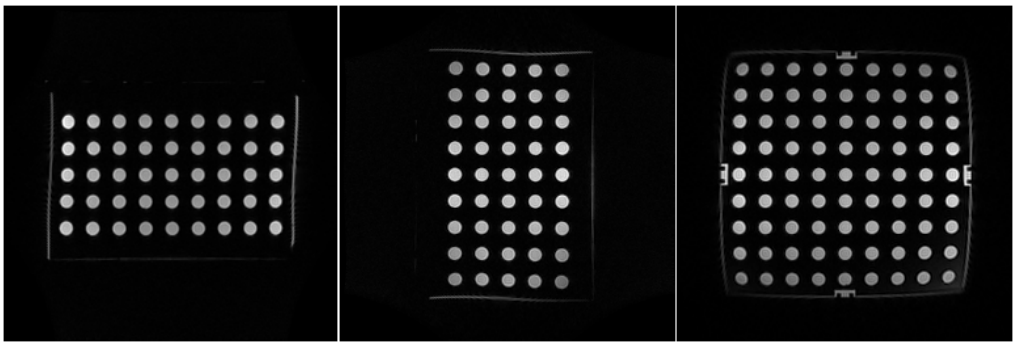

Fig. 4. MR image of the multi-orientated water-phantom in axial (left), sagittal (middle), and coronal (right) orientations.

Table 1
Center's coordinate displacement of circle holes in three directions

	No.	Min. (mm)	Max. (mm)	Mean ± S.D. (mm)
X-shift	171	-4.56	6.13	0.37 ± 0.11
Y-shift	171	-6.13	6.13	0.25 ± 0.14
Z-shift	171	-2.31	2.31	-0.10 ± 0.05

Table 2
Geometric deformation of circle holes in three anatomical slices

	No.	Min. (mm)	Max. (mm)	Mean ± S.D. (mm)
Axial	45	.93	1.10	.99 ± .005
Coronal	81	.75	1.06	.95 ± .008
Sagittal	45	.89	1.10	1.01 ± .006

Table 3
Geometric deformation of circle holes in three anatomical slices

	No.	Min. (mm)	Max. (mm)	Mean ± S.D. (mm)
Axial	45	1.00	1.19	1.04 ± .005
Coronal	81	1.00	1.20	1.05 ± .004
Sagittal	45	1.00	1.12	1.05 ± .004

Table 4
SNR of circle holes in three anatomical orientated slices

	No.	Min.	Max.	Mean ± S.D
Axial	45	77.43	117.30	90.75 ± 9.16
Coronal	81	70.88	123.13	94.49 ± 13.14
Sagittal	45	56.37	104.67	85.45 ± 10.71

SNR Contour lines of axial, coronal and sagittal planes were obtained by using a custom MATLAB program as shown in Figure 6. SNR was smaller at the center part in the left-right direction in the axial plane, especially, at the anterior and posterior sides. SNR was larger at the center part in the superior-

inferior direction in the coronal plane, especially, at the left and right sides. SNR was larger at the center part in the superior-inferior direction in the sagittal plane, especially, at the anterior and posterior sides. Generally speaking, the closer the coil is to the object, the higher the SNR. In conclusion, the SNR is in the order of coronal plane > axial plane > sagittal plane. However, the homogeneity of SNR obtained from the standard deviations is in the order of axial plane > sagittal plane > coronal plane.

4. Discussions

It has been proven that the geometric distortion highly depends on magnetic field inhomogeneity in MRI. The geometric distortion of MR image initiates at the magnet center and presents in a radial manner. The farther the region of interest from the center, the more geometric distortion created. Fortunately, the field of view (FOV) is mostly less than 24 cm × 24 cm in routine MRI examinations, excluding the chest, abdomen and pelvic examinations. It means that obvious image distortion is mostly present outside the FOV. Therefore, geometric distortion is not a crucial issue in MRI, and rarely leads to false diagnosis for examinations involving the head, neck, spine, and so on. However, the geometric distortion at the edges of MR images is always prominently present in chest, abdomen and pelvic examinations, and this may result in diagnosis failure or misinterpretation as shown in Figure 1. In order to avoid geometric distortion, it is important to make sure that the region of interest is placed as close to the magnet center as possible prior to the scan in examinations of extremities.

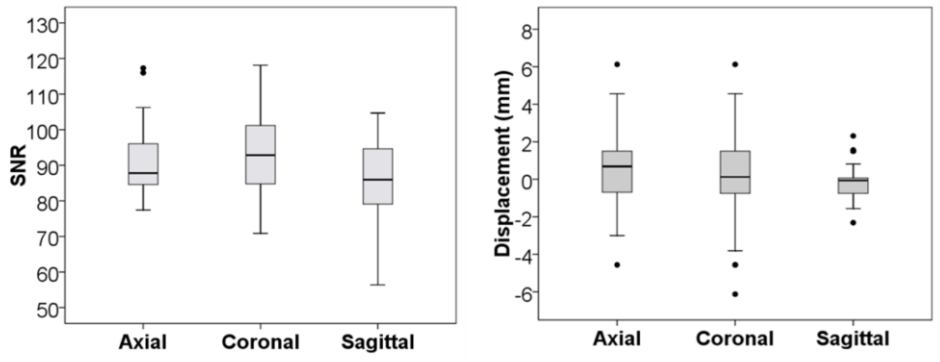

Fig. 5. Box plot of circles' SNR (left) and center-displacements (right) in three anatomical orientated slices.

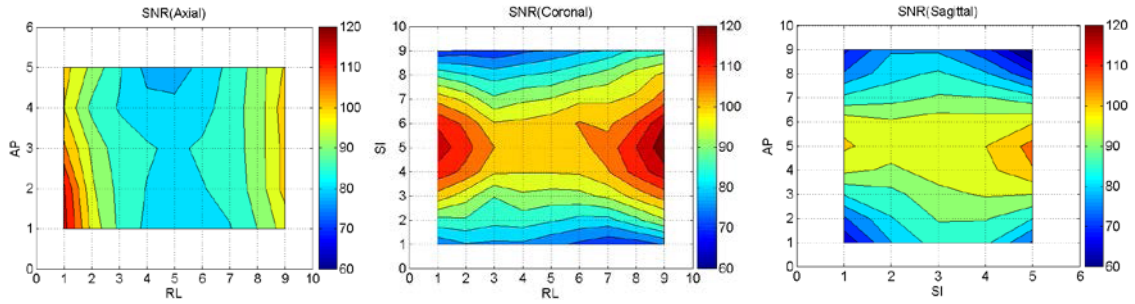

Fig. 6. SNR Contour lines of (a) axial plane, (b) coronal plane and (c) sagittal plane.

References

[1] D. Wang and D.M. Doddrell, Geometric distortion in structural magnetic resonance imaging, Current Medical Imaging Reviews **1** (2005), 49–60.
[2] P. Dammann, O. Kraff, K.H. Wrede, et al., Evaluation of hardware-related geometrical distortion in structural MRI at 7 Tesla for image-guided applications in neurosurgery, Academic Radiology **18** (2011), 910–916.
[3] L.N. Baldwin, K. Wachowicz, S.D. Thomas, et al., Characterization, prediction, and correction of geometric distortion in 3 T MR images, Medical Physics **34** (2007), 388–399.
[4] C.J. Bakker, M.A. Moerland, R. Bhagwandien and R. Beersma, Analysis of machine-dependent and object-induced geometric distortion in 2DFT MR imaging, Magnetic Resonance Imaging **10** (1992), 597–608.
[5] K. Wachowicz, T. Stanescu, S.D. Thomas and B.G. Fallone, Implications of tissue magnetic susceptibility-related distortion on the rotating magnet in an MR-linac design, Medical Physics **37** (2010), 1714–1721.
[6] J.F. Prott, U. Haverkamp, N. Willich, A. Resch, U. Stober and R. Potter, Comparison of imaging accuracy at different MRI units based on phantom measurements, Radiotherapy and Oncology **37** (1995), 221–224.
[7] T. Mizowakia, Y. Nagataa, et al., Reproducibility of geometric distortion in magnetic resonance imaging based on phantom studies, Radiotherapy and Oncology **57** (2000), 237–242.
[8] D. Wang, D.M. Dodderll and G. Cowin, A novel phantom and method for comprehensive 3D measurement and correction of geometric distortion in MRI, Magnetic resonance Imaging **22** (2004), 529–542.
[9] T. Mizowaki, Y. Nagata, K. Okajima, R. Murata, M. Yamamoto, M. Kokubo, M. Hiraoka and M. Abe, Development of an MR simulator: Experimental verification of geometric distortion and clinical application, Radiology **199** (1996), 855–860.
[10] D. Wang, W. Strugnell, G. Cowin, D.M. Doddrell and R. Slaughter, Geometric distortion in clinical MRI systems part I: Evaluation using a 3D phantom, Magnetic Resonance Imaging **22** (2004), 1211–1221.
[11] D. Wang, W. Strugnell, G. Cowin, D.M. Doddrell and R. Slaughter, Geometric distortion in clinical MRI systems part II: Evaluation using a 3D phantom, Magnetic Resonance Imaging **22** (2004), 1223–1232.
[12] R.C. Krempin, K. Schubert, et al., Open low-field MRI in radiation therapy treatment planning, International Journal of Radiation Oncology Biology Physics **53** (2002), 1350–1360.
[13] B. Peterscha, J. Bognera, A. Franssonb, T. Lorangc and R. Pottera, Effects of geometric distortion in 0.2 T MRI on radiotherapy treatment planning of prostate cancer, Radiotherapy and Oncology **71** (2004), 55–64.
[14] C. Yu, Z. Petrovich and M.L.J. Apuzzo, An image fusion study of the geometric accuracy of magnetic resonance imaging with the leksell stereotactic localization system, Journal of Applied Clinical Medical Physics **2** (2001), 42–50.
[15] D. Mah, M. Steckner, A. Hanlon, et al., MRI simulation: Effect of gradient distortions on three-dimensional prostate cancer plans, International Journal of Radiation Oncology Biology Physics **53** (2002), 757–765.